Electrochemical Impedance Spectroscopy Analysis on Steel Embedded in a Concrete Alkali Exposed on the Chloride Media.

W. Aperador[*], *E. Ruíz, A. Delgado*

School of Engineering, Universidad Militar Nueva Granada, Carrera 11 No. 101-80, Fax:+57(1) 6343200, Bogotá, Colombia.
[*]E-mail: g.ing.materiales@gmail.com

The technique of Electrochemical Impedance Spectroscopy (EIS) is used in this study to evaluate the action of chloride ion on the structural steel ASTM A 706 embedded in an alkali-activated concrete composed of: blast furnace slag, fly ash and mixing of blast furnace slag and fly ash. The study was performed by subjecting the individual to a solution containing chloride ion, simulating conditions in marine environments, the ion, added as NaCl in solution assays to 3.5%. The effect of chloride ions in concrete and its consequences, in the steel was analyzed by the scanning electron microscopy techniques. Is managed to determine the effect of chloride ions on the breakdown of the passivity of steel, and in general metal electrochemical behavior when immersed in these novel ceramic materials.

Keywords: concrete, fly ash, blast furnace slag, corrosion.

1. INTRODUCTION

Interest in the alkali activation of slag has grown significantly to date in several countries due to its superiority in mechanical and durability compared to those presented by the Portland cement properties [1-4]. The application of these new materials has been tested in pilot plants in Europe and the United States [5]. Thermal power plants generate a high rate of fly ash, because for every ton of pulverized coal burning coal in a power plant will produce about 200 kg of fly ash, pulverized coal consumption causes environmental problems due to the accumulation of fly ash in large deposits in the area close to collection areas. In most cases, you tend to use coal combustion residues replacing other natural resources and therefore provides environmental benefits [6-10]. Due to the high global production, fly ash recycling the product is necessary: therefore, currently, a mechanism of environmental control is the use in the manufacture of cement. Companies that have adapted these

technologies have the latest technology to produce cement with zero CO_2 emissions from fly ash, which ensure that their activities are made through cleaner production[11-12].

Many industries are at the forefront in building taking into account a sustainable environment, as in the manufacture of cementitious materials used industrial waste such as blast furnace slag and fly ash, reducing the amount of cement used in its composition, however it has not replaced the full use of Portland cement [13-15].

The purpose is to study the cementitious materials that have no portland cement content in order to understand their behavior individually and mixing, the tests were performed mechanical and electrochemical tests, generating good performance for concrete containing steel slag.

2. EXPERIMENTAL DETAILS

2.1 Concrete samples and specimen preparation

Table 1. Chemical composition of the steel fly ash and blast furnace slag.

Composite	Fly ash (mass %)	Granulated blast furnace slag mass %)
SiO_2	54.3	33.7
Al_2O_3	22.8	12.8
Fe_2O_3	5.8	0.48
CaO	6.9	45.4
MgO	0.8	1
Na_2O	0.9	0.12
K_2O	1.7	1.5
P_2O_5	0.7	
TiO_2	1.6	0.5
MnO	0.01	-
SO_3	0.92	-
SiO_2/Al_2O_3	3.5	2.63

Types of cementitious used:

a) Fly ash type F, coming from the power plant Termopaipa (Boyacá Colombia), whose chemical composition is recorded in Table 1. The ignition loss was 6.54% of the total mass determined by calcination of the sample at 1000 °C, value associated mainly remnants of unburned coal. In addition, we assessed the proportion of reactive silica from fly ash following the procedure described in the standard UNE 80-225-93, obtaining a value of 46.15% by mass [16].

b) Steel blast furnace slag (GBFS) with chemical composition shown in Table 1, ratios of basicity (CaO + MgO / SiO_2 + Al_2O_3) of 1.0 and quality (CaO + MgO + Al_2O_3 / SiO_2 + TiO_2) 1.73. As alkaline activator, a solution of sodium silicate at a concentration of 5% Na2O, expressed as percent by weight slag (ASTM C 989-99) was used [17].

The aggregates are gravel with maximum size of 17 mm, specific gravity of 3.12 and absorption of 1.6%; and river sand with specific surface area of 2380 kg / m^3 and 3.0% absorption. After the cementitious materials and aggregates, were prepared concrete 400 kg per m3 of concrete and in relation 0.5, water / cement [18-19].

For the study, three types of concrete samples were formed 100% of steel slag (GBFS); 100% Fly Ash (FA); and a mixture of blast furnace slag and fly ash at 50%. Table 2 shows the type of specimen and their composition [20].

Table 2. Type and Conformation of concrete specimens.

Class	Composition
G100	100% GBFS
FA100	100% Fly ash
G50-FA50	50% de GBFS + 50% Fly ash

2.2 Electrochemical test

For the electrochemical evaluation cylinder were produced of diameter of 76.2 mm by 76.2 mm high, with a structural steel rod ASTM A 706 placed in the centre of the specimen; the reinforcing steel diameter were 6.35mm. Figure 1 shows the corresponding assembly, details such as the length of exposed steel (50mm), the segments of the rebar that were painted and the location of an epoxy at the interface was observed. The top of the concrete specimens were protected with the epoxy material to prevent entry of chlorides preferred for the interface steel / concrete [21]. The concretes obtained from mixtures of: steel slag and fly ash alkali activated were cured at a relative humidity of 90% for 28 days, before the development of the various tests. For concrete obtained with fly ash is initially activated in an oven at 80 ° C for 24 hours, and then cured in a pool for 28 days.
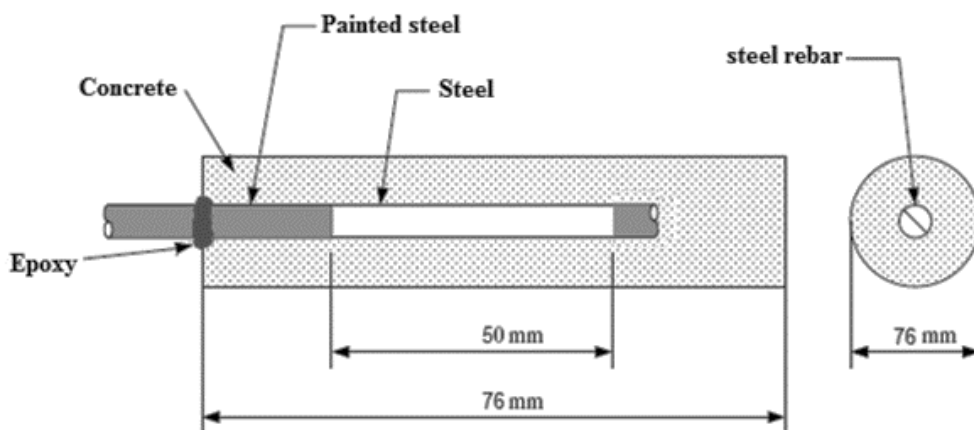

Figure 1. Schematic diagram of the sample reinforced concrete.

For electrochemical characterization, a potentiostat / galvanostat model Gamry PCI 4 was used by the technique of electrochemical impedance spectroscopy. The cell was comprised of a counter electrode of graphite (which is not embedded in concrete) reference electrode $Cu/CuSO_4$ and structural steel ASTM A 706 with display area of 10 cm^2 as a working electrode.

Figure 2 shows the experimental setup for the development of electrochemical characterization was observed. During the development of the analysis, the various specimens were immersed in a tank containing distilled water. Nyquist plots obtained by frequency sweeps between 0.01 Hz and 100 kHz with 10 mV amplitude sinusoidal signal. The measurement of open circuit potential was performed until stabilization a time of 3.33 hours.

Electrochemical measurements for the three types of concrete and listed in Table 2 taken every month until 6 months. All samples were subjected to the corrosion process by immersion in a solution of 3.5% NaCl, extracted only by the time required to practice the various analyses.
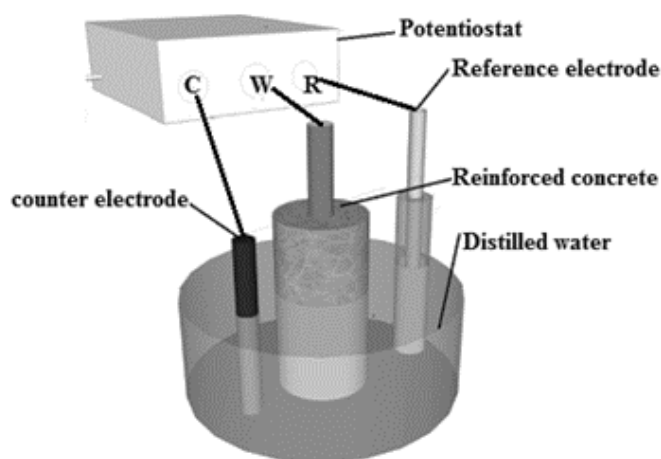
Figure 2. Schematic of the experimental setup for electrochemical measurements.

2.3 Characterisation tests

For the characterization of the chloride ion, In this electrochemical assay, a cylindrical specimen of concrete of 50 mm thickness and 100 mm diameter is placed between two cells that serve as reservoirs, and between which are embedded metal electrodes through which a voltage of 60V is applied for 6 hours. One of the cells is filled with a 0.3 N NaOH solution, which serves as an anode while the other cell with a 3.0% NaCl solution serves as a cathode. The curved surface of the cylinder is coated with an epoxy resin that prevents the sample loses its saturation condition during the test, the sample being previously required condition as specified in the standard. In this experiment, the electrical conductivity of the concrete was determined providing a rapid indication of the resistance to penetration of chloride ion, this is performed on cylindrical samples 3.81 cm x 7.62 cm after 28 days of curing. For determination of mechanical properties was performed under ASTM C109; on a universal Instron machine. Cylindrical concrete 3 cm x 6 cm were used after curing time, were used to test the materials for compressive strength according to ASTM C 42-04 Standard.

Using the technique of scanning electron microscopy (SEM), high resolution (Philips XL 30 FEG) equipped with a light-sensitive element (EDX system) with a resolution of 1 nm at 30 kV determined the morphology of cementitious additionally this technique was used to characterize the morphology of the corrosion products.

## 3. RESULTS

3.1 Characterization of raw materials

Morphological characterization of the raw material, was performed by SEM techniques allowed identification of its morphology. In Figure 3, it is observed that fly ash studied show a typical microscopic appearance with spherical particles of various sizes, micro-spheres, cenospheres and pleurosferas. These fly ashes have a high proportion of irregular sponge-like particles that provide a high porosity, and presented normally grouped together to form agglomerates. In addition to spherical particles can be observed irregularly shaped particles mainly quartz particles of unburned particles of calcite and anhydrite particles [22].

The formation of spherical particles is due to the influence of elevated temperatures on the boiler and a series of complex physical and chemical changes that occur in the particles, the most notable is the rapid conversion to spherical forms as a result of surface tension forces acting during fusion to minimize the surface free energy. The abundance of glassy phase in the fly ash is due to rapid cooling [23]. The particles emerging from the flame carried by the gas stream and quickly passed to a lower temperature regime where they are cooled to a glassy solid state. The cooling rate depends on the particle size: the larger particles cool more slowly allowing crystallization within the interior (center portion in the figure 3). In addition, some of inflated particles explode and form small molten droplets. Other particles are cooled in the same way that the solid particles when they finally leave the flame and remain as hollow spheres with variations in wall thickness.
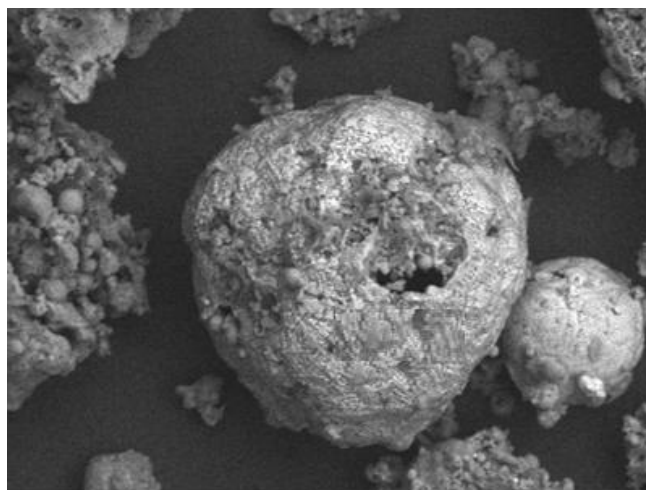
Figure 3. Forms of fly ash used as cement, the particular shape spherical observed by SEM

The steel slag is a byproduct of the manufacture of cast iron is separated from it in the liquid state (melted) in the blast furnace process [24]. The type of GBFS, is quenched with air (pelletizing) a glassy product which gives a cementitious powder milled latent hydraulic properties is obtained. The hydraulic activity of slag, essentially depends on its structure, which is related to the chemical composition and thermal history and influences the amount of glass phase therein. The activating solutions incorporated may accelerate the solubilization of the slag, promote the formation of stable hydrates of low solubility and the formation of a compact structure with these hydrates.
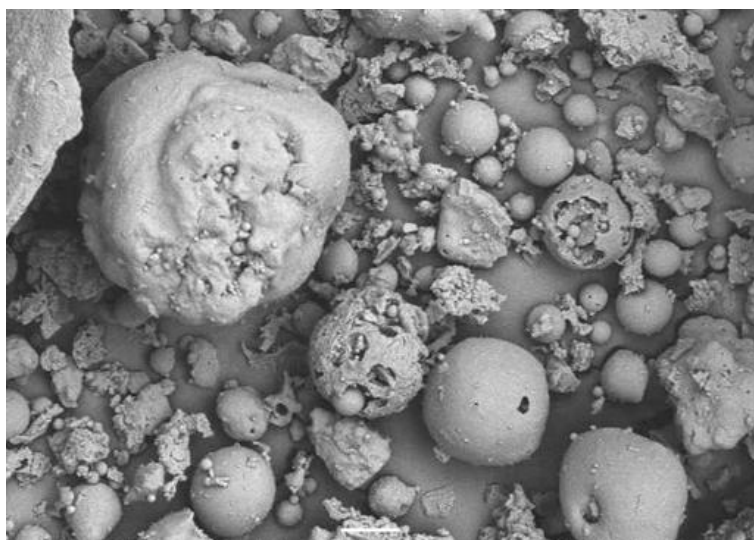
Figure 4. Micrograph of steel slag used as cement, it can be seen how the pellets obtained after the cooling process

3.2 Mechanical evaluation

Was evaluated the compressive strength of concrete samples alkali-activated at 28 days of curing.
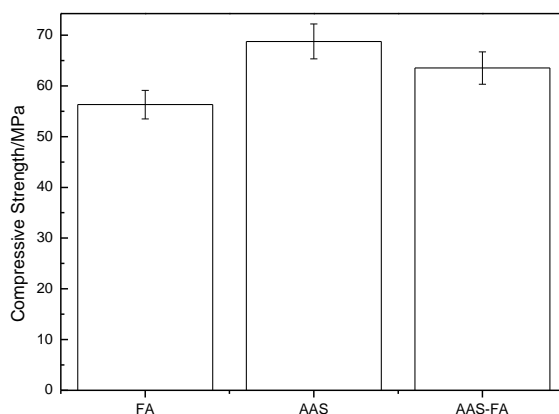
Figure 5. Compressive strength of the alkali-activated concrete, with and without mixture of cementitious material

These results are shown in Figure 5 wherein it is seen that the highest value of compressive strength for concrete obtained with 100% slag, for the test piece which has a percentage of 50% of slag and fly ash shows a decrease compressive strength but this loss is not significant since it is within the error bar, because it is comparable to the measurement obtained at 28 days of curing concrete GBFS [25]. The values of compressive strength of the fly ash concrete generates a resistance of 55.23 MPa. This behaviour is related to the particle size of the fly ash, because of its large size the compressive strength is decreased, further the activity of the ash pozzolan activation generates evolves over time, showing better performance after 90 days .

3.3 Evaluation of Rapid Determination of the Chloride Permeability

Chloride ion permeability of the concrete is yield by calculating the electric current passing through them. The measurements were performed after 28 days of curing. In Figure 6, the behaviour of the specific analyses based transferred load is observed here is obtained that the specific GBFS has a permeability to chloride; compared to the other mixtures [26]. This is because in this process has been obtained clogged pores; process can also be observed in combination with concrete mixtures where an increase is observed charge passed, because the behaviour is similar to 100% GBFS for fly ash concrete obtained with the transmitted load increases by 52% compared to the specific GBFS, although can be classified as low chlorine ion permeability. With permeability test chlorides can be determined indirectly concrete resistivity where in turn measure the resistivity of concrete is used to interpret the value of the corrosion rate, as it is inherently related to the moisture content of the concrete. The rapid test for chloride ion permeability, is essentially a measure of the electrical conductivity depends on the pore structure and chemistry of the solution thereof. For a given applied voltage and specimen size, initial current recorded can be taken as representative of the electrical conductivity of the sample. It is noted that concrete containing fly ash have a higher electrical conductivity than the GBFS concrete [27].
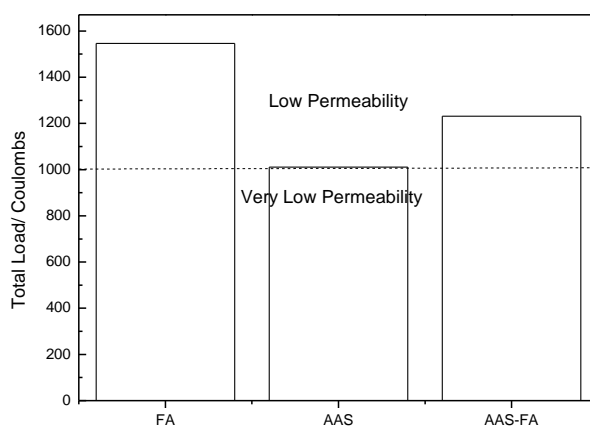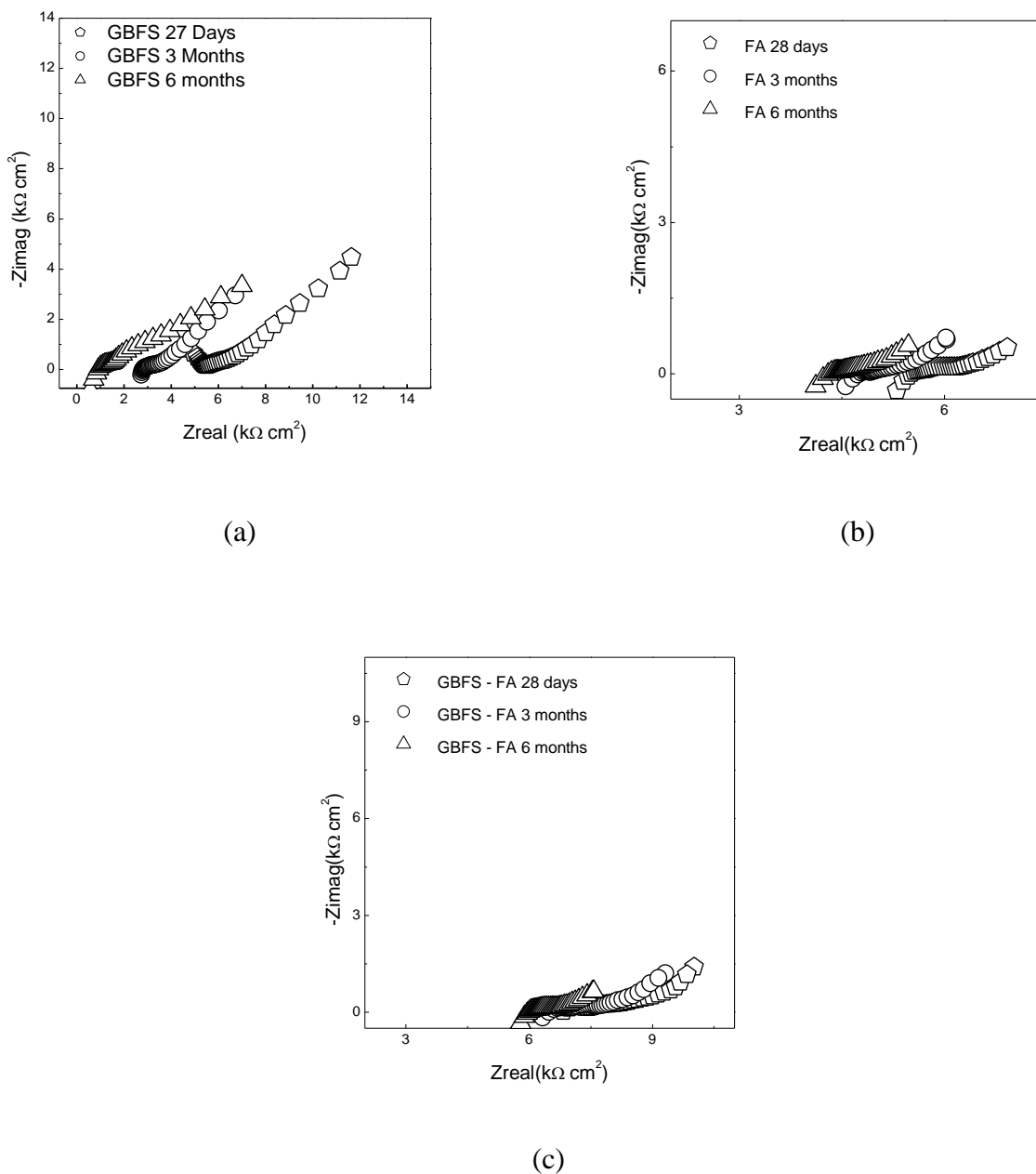

Figure 6. Charge transferred in different alkali-activated concrete mixtures.

*3.4 Electrochemical Impedance Spectroscopy*

(a)

(b)

(c)

Figure 7. Nyquist diagram for the alkali-activated concrete, a) steel slag, b) fly ash c) mixture of fly ash and blast furnace slag.

In Figures 7 the Nyquist diagrams corresponding to the alkali activated and exposed to a solution containing chloride ion after 28 days of curing time and even by a specific 6 months, in the three mixtures was observed that the phenomenon is similar, because a decrease in all electrochemical parameters is obtained; especially the solution resistance and polarization resistance in the first 3 months of evaluation, high attenuation is due to the entry of chloride ion in concrete. The same

behaviour for other levels studied in which a reduction is due to the leftward shift of each of the Nyquist diagrams observed.

To model the elements found in this system analyzed, the circuit shown in Figure 8 was used, it is used to electrochemically explain the effect of chloride ions on the breakdown of the passivity of steel, this model is the best fit because the first resistance is the opposition of the ions of the solution entering the concrete this value is small for the first few levels because the amount of ions in the early levels is minimal, therefore come easily, then in the following these particular levels are saturated solution aggressive therefore this value is increased, then a resistor (R1) is shown which is generated at the interface of the solution and concrete aggregates then a resistor (R1) which is generated at the interface of the solution and aggregates of the concrete. The value of this resistor varies depending on the rated level (3 to 6 months), because in the first 3 months increased resistance of ions is generated when passing through the aggregate, this resistance begins to decrease because the concrete resistivity begins to drop when chloride ion is entered into the system, in the same interface is parallel to the element R1 constant phase CPE_1 which acts as a condenser provided surface imperfections found on this interface [28]. This value of the CPE for each of the cases is higher because this ion generating another path which is represented by the found resistance between the concrete and the passive layer of the steel, the value of polarization resistance (Rp) is shrinking due to the opposition in the early levels is higher due to the passivation layer found in this system this layer begins to be compromised after a certain amount of chlorine ions have come to the interface, ie as the percentage of chlorine is increased by this interface; Due to this the value of polarization resistance is decreasing, indicating an increase in the corrosion rate, the element of constant phase corresponding to the interface which is parallel to the polarization resistance shows a drop of this parameter this phenomenon is to be expected in this case because this element at each level offers a greater passage of ions due to deterioration worn on the steel surface.
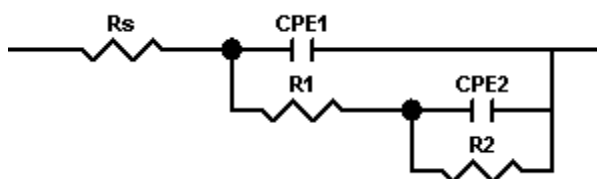
**Figure 8**.Circuit to fit the impedance data of steel embedded in alkali-activated concrete.

3.5 SEM

In the figure 9, the SEM micrographs are observed the superficial microstructure of the steel embedded in the alkali-activated slag, after 6 months of evaluation. These images correspond to the corrosion products which are deposited on the steel surface, it is clearly observed that the whole surface has an oxide layer. Furthermore at 500X, the corrosion products (Magnetite and Wuestite) are superimposed due to a zone in a state denominated homogeneous owing to the absence of cracks in the sector.
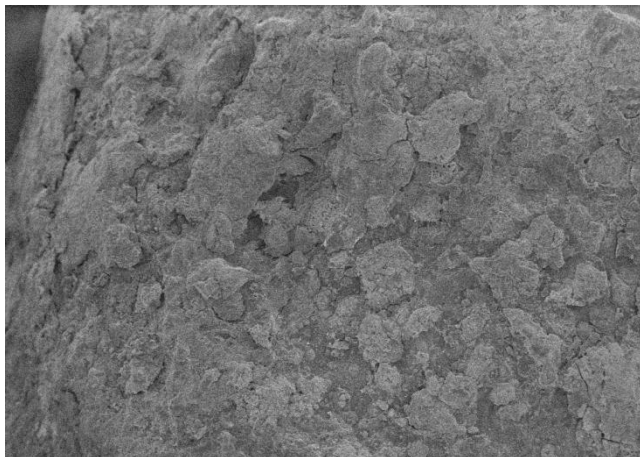
Figure 9. Microscopic observation (500X magnification) of the steel in contact with the mixture of the steel alkali-activated slag, subjected during 6 months in chloride ion.

In the figure 10 is observed the micrographs of the steel surface embedded in the concrete alkali-activated with fly ash. It can be observed at 500X of magnification the generation of a cracks due to movement of the corrosion products that diverge of the all sides, therefore, a space in the junction is observed in all of them. In the upper left of the micrograph is observed a zone where is exhibited a large number of intertwined cracks forming light and dark areas, generating by the movement of the corrosion products which are in rearrangement. By EDS is obtained that the corrosion products are Magnetite, Wuestite and Goethita, which are in circulation on the steel surface thus there light and dark areas.
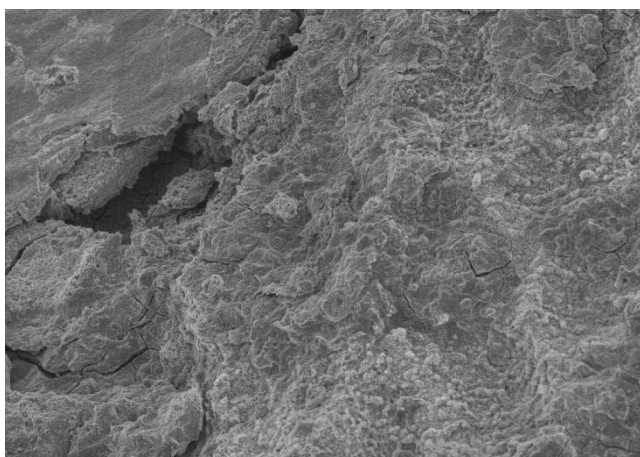
Figure 10. Microscopic observation of the steel in contact with the alkali-activated slag concrete subjected to 6 months in an electrolyte with chloride ion content.

In the figure 11, are observed the corrosion products that are presented on the steel surface of the concrete generated by the slag and fly ash mixture, after 6 months of exposition in a solution with chloride ion. As the GBFS an FA concrete is found the same corrosion products (Magnetite, Wuestite

and Goethita), in the 500X micrographs is noticed zones with porous aspect caused by corrosion phenomenon in where the chloride ion enters and generates this type of degradation. In addition is observed a series of cracks which are similar to those found in the FA, the difference between these cracks in this material is that the cracks are smaller in diameter. The generation of these cracks is due to the previous analysis and the movement of the corrosion products on the steel surface [29].
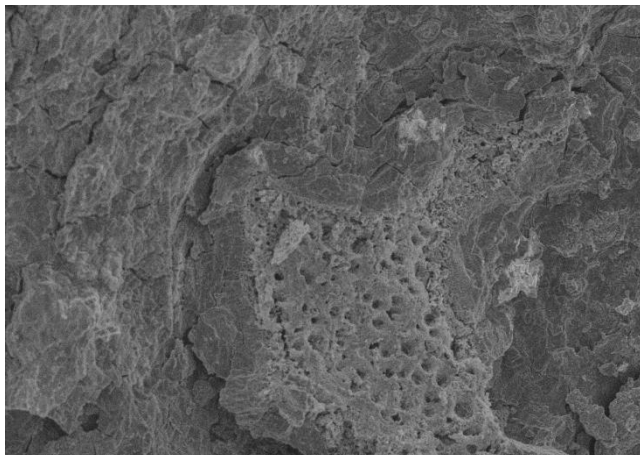
Figure 11. Microscopic observation of the steel in contact with the GBFS concrete subjected to 12 months in a solution without chloride: a) 500X, b) 1000X y c) 2000X.

4. CONCLUSIONS

Using these alkaline cements based on slag and fly ash in where are differentiated among them in the starting situation: composition and alkalinity. The application of these materials can be comparable to Portland cement, with the advantage that its production has a significant reduction in emissions of greenhouse gases. These cementitious working separated as a mixture form generate good mechanical and fast setting; but these properties depend on the selected source materials and the processing conditions. To highlight how the nature of raw materials affects the progress and the development of chemical reactions, it is done a simultaneous discussion of the differences that characterize materials based on slag and the fly ash.

References

1. M. Hajian, A. Abdollah-zadeh, S.S. Rezaei-Nejad, H. Assadi, S.M.M. Hadavi, K. Chung, M. Shokouhimehr, *Appl Surf Sci*, 308 (2014) 184
2. A. Fernández-Jiménez, A. Palomo, I. Sobrados, J. Sanz. *Micropor. Mesopor. Mater*. 91 (2006) 111
3. F. Puertas, M. Palacios, T. Vázquez. *J. Mater. Sci*. 41 (2006) 3071

4. M. Palacios, F. Puertas. Effect of carbonation on alkali-activated slag paste. *J. Am. Ceram. Soc*. 89 (2006) 3211
5. V. Saraswathy, H.-W. Song. *Electrochim. Acta*, 51 (2006) 4601
6. P. Duxson, A. Fernández-Jiménez, J.L. Provis, G.C. Lukey, A. Palomo, J.S.J. van Deventer. *J. Mater. Sci*. 42 (2007) 2917
7. D. Panias, I.P. Giannopoulou, T. Perraki. *Colloid. Surface. A: Phys. Eng. Aspects*. 301 (2007) 246
8. M. Criado, A. Fernández-Jiménez, A.G. de la Torre, M.A.G. Aranda, A. Palomo. *Cement Concrete Res*. 37 (2007) 671
9. V. Živica. *Constr. Build. Mater*. 21 (2007) 1463
10. M. Palacios, F. Puertas. *Cement Concrete Res*. 37 (2007) 691
11. G. Qiao, J. Ou. *Electrochim. Acta* 52 (2007) 8008
12. H.-W. Song, V. Saraswathy. *Int. J. Electrochem. Sci*., 2 (2007) 1.
13. M. Criado, A. Fernández-Jiménez, A. Palomo, I. Sobrados, J. Sanz. *Micropor. Mesopor. Mater*. 109 (2008) 525
14. D.M. Bastidas, A. Fernández-Jiménez, A. Palomo, J.A. González. *Corros. Sci*. 50 (2008) 1058
15. F. Puertas, M. Palacios, A. Gil-Maroto, T. Vázquez. *Cement Concrete Comp*. 31 (2009) 277
16. C. Duran Atiş, C. Bilim, Ö. Çelik, O. Karahan. *Constr. Build. Mater*. 23 (2009) 548
17. W. Aperador, R. Mejía de Gutiérrez, D.M. Bastidas. *Corrosion Sci*. 51 (2009) 2027
18. R. Montoya, W. Aperador, D.M. Bastidas. *Corrosion Sci*. 51 (2009) 2857
19. J.E. Oh, P.J.M. Monteiro, S.S. Jun, S. Choi, S.M. Clark. *Cement Concrete Res*. 40 (2010) 189
20. D. Ravikumar, S. Peethamparan, N. Neithalath. *Cement Concrete Comp*. 32 (2010) 399
21. E.I. Diaz, E.N. Allouche, S. Eklund. *Fuel*. 89 (2010) 992
22. M. Komljenović, Z. Baščarević, V. Bradić. *J. Hazard. Mater*. 181 (2010) 35
23. M. Criado, A. Fernández Jiménez, A. Palomo. *Cement Concrete Comp*. 32 (2010) 589
24. P. Garcés, L.G. Andión, E. Zornoza, M. Bonilla, J. Payá. The effect of processed fly ashes on the durability and the corrosion of steel rebars embedded in cement-modified fly ash mortars. Cement Concrete Comp. 32 (2010) 204-210
25. A. Fernández-Jiménez, J.M. Miranda, J.A. González, A. Palomo. *Mater. Construc*. 60 (2010) 51
26. İ. Bekir Topçu, A. Raif Boğa. *Mater. Design*. 31 (2010) 3358
27. Y. Fu, L. Cai, W. Yonggen. *Constr. Build. Mater*. 25 (2011) 3144
28. S.P. Arredondo-Rea, R. Corral-Higuera, M.A. Neri-Flores, J.M. Gómez-Soberón, F. Almeraya-Calderón, J.H. Castorena-González, J.L. Almaral-Sánchez. *Int. J. Electrochem. Sci*., 6 (2011) 475
29. A.A. Naqvi, M. Maslehuddin, M.A. Garwan, M.M. Nagadi, O.S.B. Al-Amoudi, Khateeb-ur-Rehman, M. Raashid. *Nucl. Instrum. Meth. Phys. Res. Section B*: *Beam Interactions Mater. Atom*. 269 (2011) 1